Fuel Processing Technology 167 (2017) 50–60

Contents lists available at ScienceDirect

Fuel Processing Technology

journal homepage: www.elsevier.com/locate/fuproc

Research article

Selective conversion of bio-ethanol to propene over nano-HZSM-5 zeolite: Remarkably enhanced catalytic performance by fluorine modification

Ni Zhang, Dongsen Mao *, Xiaolong Zhai

Research Institute of Applied Catalysis, School of Chemical and Environmental Engineering, Shanghai Institute of Technology, Shanghai 201418, PR China

ARTICLE INFO

Article history:
Received 23 December 2016
Received in revised form 11 June 2017
Accepted 24 June 2017
Available online xxxx

Keywords:
Bio-ethanol
Propene
Nano-HZSM-5 zeolite
Fluorine modification

ABSTRACT

A series of fluorinated nano-HZSM-5 zeolite catalysts were prepared by impregnating with NH_4F solutions of various concentrations and applied to the selective conversion of bio-ethanol to propene at 500 °C, atmospheric pressure, and WHSV of 10 h^{-1}. The characterizations by XRD, TEM, N_2 adsorption, ICP-OES, EDX, ^{27}Al MAS NMR, NH_3-TPD, Py-IR, and TG techniques revealed that fluoride treatment had a major effect on the channel structure together with the acidic properties. The newly formed mesopores increased the coke tolerance capacity and reduced the probability of coke formation by facilitating mass transfer, and the weakened acidity suppressed the formation of coke. Hence, fluorine modification with suitable content (20 wt%) significantly enhanced the selectivity of propene as well as the catalytic stability. In addition to coke, elimination of aluminum in the zeolite framework was also an important reason for the deactivation of fluorinated nano-HZSM-5 zeolite catalyst.

1. Introduction

Propene, as a basic raw material, is widely used in chemical industry. Currently, propene is principally produced by steam cracking of naphtha, fluid catalytic cracking (FCC), MTO/MTP (methanol to olefins/propene), olefins disproportionation and propane dehydrogenation. Unfortunately, the aforementioned processes not only heavily depend on the fossil resources, but also cannot meet the huge demand for the production of propene derivatives such as propene oxide, polypropene and acrylonitrile. Considering the petroleum crisis coupled with environmental protection, developing new routes for "green propene" are highly required. Since ethanol can be obtained from renewable biomass sources, the direct conversion of ethanol to propene (ETP) process would tremendously decrease oil crisis as well as carbon emissions [1–3].

While many catalytic systems have been investigated, HZSM-5 zeolite catalyst remains the most promising system for the ETP reaction [4]. Unfortunately, conventional HZSM-5 zeolite catalyst not only exhibits a relatively low selectivity of propene, but also usually leads to diffusion limitation due to the microporous nature of zeolite, which deactivates the zeolite catalyst quickly [5,6]. Introducing mesopores or macropores into zeolite structure [5–8] and reducing the size of HZSM-5 crystals [9–12] have been proved as two possible routes to enhance the mass transfer rate thus improving the catalyst stability in the conversion of ethanol to hydrocarbons. For example, Ramasamy et al. [5] compared the catalytic performance of conventional and hierarchical HZSM-5 zeolites with similar Si/Al_2 ratios in the ethanol conversion at 360 °C and found that the catalytic lifetime of the hierarchical HZSM-5 is approximately 2 and 5 folds larger than that of conventional HZSM–5 at the Si/Al_2 ratios of 40 and 140, respectively. Meng et al. [10] investigated the effect of H-ZSM-5 (Si/Al_2 = 70) crystallite sizes (500, 250 and 100 nm) on the ETP reaction at 500 °C and found that the small-sized catalyst shows better stability than the larger ones, which can be attributed to its larger pore volume, more secondary pores, shorter channels, and reduced diffusion path lengths. Very recently, Lakiss et al. [13] reported that reducing the zeolite crystal size to nanometers is more efficient than adding macropores or mesopores to micron-sized zeolites in the conversion of ethanol to hydrocarbons at 350 °C.

On the other hand, numerous studies have indicated that the catalytic performance of the HZSM-5 zeolite in the ETP process is also strongly dependent on the acidity (strength and number of acid sites) of the zeolites [1–4]. In this context, many efforts have been made to improve the catalytic performance for ETP reaction by adjusting the acidic property of HZSM-5 zeolite through various procedures, such as the modifications with various metals [14–16] and phosphorus [17,18], alkali treatment [7], co-modifications with alkaline and phosphorous [6], and the utilization of HZSM-5/SAPO-34 composite zeolites [19,20].

Luckily, it is worth mentioning that fluorine modification can simultaneously modulate the acidity and the pore characteristics of zeolite

* Corresponding author.
E-mail address: dsmao@sit.edu.cn (D. Mao).

http://dx.doi.org/10.1016/j.fuproc.2017.06.028
0378-3820/

catalysts, such as β, Y, and ZSM-5 [21–24]. The fluorination often provokes dealumination, and further affects the acidic characteristics of the zeolites. At the same time, the catalytic performance was improved obviously on the fluorinated catalysts with optimum content in some reactions [21–24]. However, there has been no detailed study on the fluorinated HZSM-5 zeolite catalysts applied to the ETP reaction, as far as we know.

Therefore, in this paper, a commercial nano-sized HZSM-5 zeolite was modified by fluorine to further improve its catalytic performance in the ETP process for the first time. Based on the results, the higher propene selectivity and especially the markedly enhanced catalytic stability were obtained over the nano-HZSM-5 zeolite by modification with suitable content of fluorine. Moreover, the correlation between the physicochemical properties of the studied catalysts and their catalytic performances for the ETP reaction was also discussed in depth.

2. Experimental

2.1. Catalyst preparation

The fluoride modified nano-HZSM-5 zeolite was prepared by an isovolume impregnation method. The NH_4F solutions of various concentrations were added dropwise into the commercial nano-sized HZSM-5 zeolite power (Si/Al molar ratio of 19, average crystal size of 80 nm), provided by Zibo Tengjin Energy Saving Technology Co., Ltd., China. After ultrasonic treatment at room temperature for 30 min, the obtained sample was laid at room temperature for 3 h, dried at 110 °C overnight and calcined in air at 500 °C for 4 h. In terms of the content of fluorine (wt%) in the sample, the NH_4F-modified HZSM-5 catalysts were denoted as HZ-F-5, HZ-F-10, HZ-F-15, HZ-F-20, and HZ-F-25 respectively, and the unmodified sample was named as HZ.

2.2. Catalyst characterization

X-ray diffraction (XRD) data were acquired using a PANalytical X'Pert diffractometer operating at 35 kV, and 25 mA with Cu-Kα radiation source in the 2θ range of 5–50°. The integrated intensity of the signals at $2\theta = 22–25°$ was used to evaluate the relative crystallinity of HZSM-5 zeolites. The bulk Si/Al molar ratios of the samples were determined by ICP-OES (PerkinElmer Optima 7000DV). ^{27}Al MAS NMR spectra were recorded on a Bruker Avance-III 600 spectrometer. Chemical shifts were referenced to a 1.0 mol/L $Al(NO_3)_3$ aqueous solution. The spectra were determined at 156.41 MHz with a spinning rate of 14 kHz, a recycle delay of 1.0 s and a pulse width of 3.0 μs.

An energy dispersive X-ray (EDX) spectrometer from Hitachi (S-3400N) was used to examine the content of fluorine remaining in the modified catalysts using the X flash detector 4010 (Bruker ALX) [22], operating at 15.4 kV in vacuum. The sample was prepared by loading a small quantity of ZSM-5 powder onto a conducting carbon tape adhered to a standard stud. Transmission electron microscopy (TEM) was performed with a TECNAI G^2 S-TWIN electron microscope operating at 200 kV.

A Micromeritics ASAP 2020 HD88 equipment was used for nitrogen adsorption measurements at −196 °C. Prior to measurement, the samples were outgassed at 200 °C for 13 h under vacuum. Total surface area was obtained by the Brunauer-Emmett-Teller (BET) equation, and the micropore area and volume were calculated according to the t-plot method. The external area was acquired by subtracting the micropore area from the total BET surface area. The average pore size was measured by BJH method.

The acidic properties of the catalysts were studied by temperature programmed desorption of NH_3 (NH_3-TPD) and the Py-IR spectra. The NH_3-TPD measurement was carried out on a conventional apparatus equipped with a thermal conductivity detector (TCD). The samples (0.1 g) were pretreated at 500 °C for 1 h in a N_2 stream. Then, they were cooled down to room temperature and saturated with ammonia (10 mol% in N_2). The physisorbed NH_3 was outgassed at 100 °C for 1 h in a N_2 stream (50 mL min^{-1}). Finally, the desorption of NH_3 was carried out from 100 °C to 550 °C at a heating rate of 10 °C per minute in the N_2 stream and determined by TCD. The Py-IR spectra were recorded on a Nicolet 6700 infrared spectrometer with a resolution of 4 cm^{-1}. The samples were pretreated at 400 °C for 3 h under vacuum (10^{-2} pa). Pyridine vapor was adsorbed at room temperature for 30 min, and then pyridine was desorbed by evacuation of the sample at the desired temperature for 1 h. Finally, the IR spectra of the pyridine adsorbed on the samples were recorded.

A thermogravimeric (TG) analysis was operated on a Shimadzu DTG-60H equipment with the spent samples from 30 to 800 °C under flowing air at a rate of 25 mL min^{-1} and a constant ramping rate of 10 °C min^{-1}. The coke content of the spent catalyst was determined according to weight loss between 400 and 700 °C [6].

2.3. Catalyst testing

The catalytic performance of the parent and modified HZSM-5 zeolite catalysts was evaluated for the selective conversion of bio-ethanol to propene in a conventional continuous flow fixed-bed reactor made of stainless steel (inner diameter of 6 mm, effective length of 20 cm) under the reaction conditions of 500 °C, atmospheric pressure and WHSV of ethanol = 10 h^{-1}. The catalyst weight was 0.3 g and sieved in the range of 40–60 mesh. The mixture of pure ethanol and water (90 vol% ethanol) was used as feedstock and pumped through a small-flow feed pump. The reaction products were analyzed by an online gas chromatograph (Agilent 6820) with a FID and a HP-Plot-Q capillary column. The temperature of the effluent line was constantly maintained at 180 °C in case of the possible condensation of heavier hydrocarbons.

The conversion of ethanol and selectivity of products were calculated as follows:

Conversion of ethanol % = number of converted ethanol moles/number of introduced ethanol moles × 100.

Selectivity of product i % = $(v_iC_i / \sum v_iC_i) \times 100$, where v_i is the number of carbon atom, and C_i is the molar concentration of the ith product.

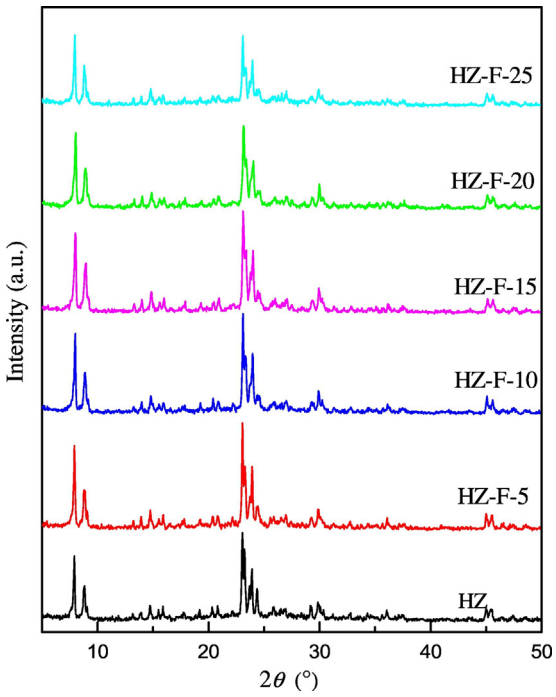

Fig. 1. XRD patterns of different samples.

Table 1
Porosity, relative crystallinity, Si/Al ratio and F content of different samples.

Sample	Specific surface area ($m^2 \cdot g^{-1}$)			Pore volume ($cm^3 \cdot g^{-1}$)			D_p[a] (nm)	RC[b] (%)	Si/Al ratio[c]	F[d] (wt%)
	Total	Micropore	External	Total	Mesopore	Micropore				
HZ	326	226	100	0.19	0.07	0.12	2.30	100	18.1	–
HZ-F-5	343	198	145	0.21	0.11	0.10	2.40	107	22.7	5.7
HZ-F-10	331	121	210	0.21	0.14	0.07	2.56	103	23.1	16.4
HZ-F-15	332	94	238	0.23	0.18	0.05	2.74	108	22.0	30.6
HZ-F-20	340	68	272	0.25	0.21	0.04	2.88	85	18.4	32.0
HZ-F-25	336	62	274	0.27	0.23	0.04	3.24	73	19.0	33.1

[a] Average pore diameter.
[b] Relative crystallinity calculated from XRD patterns.
[c] Determined by ICP-OES.
[d] Determined by EDX.

3. Results and discussion

3.1. Characterization of the catalysts

3.1.1. Structural and textural properties

As shown in Fig. 1, all the zeolite samples retained their reflection lines corresponding to the typical MFI topology after fluorine modification. However, some changes of the relative crystallinity had been found with increasing the concentration of the NH_4F solution. More specifically, when the content of fluorine was ≤15 wt%, the relative crystallinity increased to a certain extent (Table 1), which can be due to the leaching of the amorphous or less crystalline material remaining in the channel from the synthesis by HF produced by the decomposition of NH_4F [25]. While the relative crystallinity of HZ-F-20 and HZ-F-25 respectively decreased to 85% and 73% with higher amounts of F, indicating that some structural damage has occurred. This phenomenon was also reported by other researchers [21,22]. The probable reason was that highly concentrated NH_4F solution partially extracted aluminum from the zeolite framework [26], which was illustrated by ^{27}Al MAS NMR measurement (see below).

Fig. 2 presents the TEM images of the representative HZ and HZ-F-20 samples. It can be seen that, compared with the pristine zeolite with a relative smooth surface morphology, the fluorinated HZSM-5 presented some etched crystals and defects. The rough surface, fragile particles and the gap between particles may contribute to form the new mesopores which increase the external surface area [27], matching well with the results of N_2 adsorption-desorption measurement (see below).

According to the ICP-OES analysis (Table 1), the Si/Al ratio increased to a certain extent from the parent HZ to the modified samples with F content ≤ 15 wt%, suggesting that the Al atoms had been preferentially extracted from zeolite frameworks [28,29]. When treated with higher NH_4F solutions (20 and 25 wt%), however, the Si/Al ratio respectively decreased to 18.4 and 19.0, close to its parent value (18.1). This is probably due to the fact that the more concentrated NH_4F solutions can simultaneously extract Si and Al atoms in zeolites, which results in the decreased selectivity in dealumination.

As shown in Table 1, compared with the parent HZ, the external surface areas of the fluorinated samples increased significantly and progressively with increasing F contents. It demonstrated the generation of new mesopores by fluorine treatment and the N_2 physisorption isotherms further proved the existence of mesoporous structure as shown in Fig. 3A. As seen, the parent zeolite HZ showed a type I (IUPAC) isotherm with sharp uptakes in the adsorption capacity at low pressure and ended with a plateau at higher relative pressure [30]. Upon fluorine treatment, the isotherms changed obviously from type I to type IV with a H3 hysteresis loop [31]. The special hysteresis loop appearing at $P/P_0 = 0.1–0.4$ was a result of a phase transition of the adsorbed N_2 from a disordered "fluid" phase to a more ordered "crystalline" like phase [32]. The larger hysteresis loop in the relative pressure range of 0.5–1.0 corresponded to the inter-crystalline mesopores formed by the accumulation of nano-crystallites [10,31].

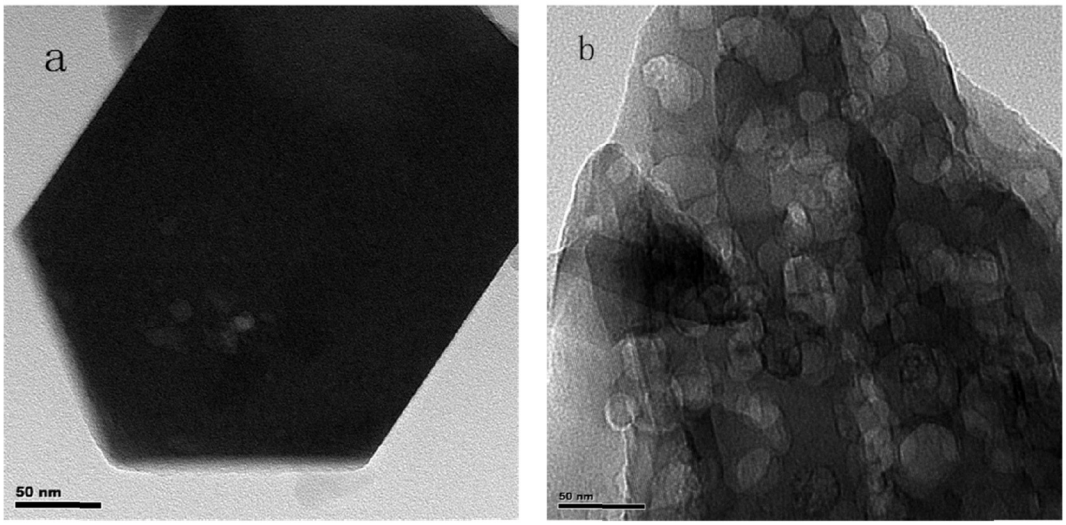

Fig. 2. TEM images of HZ (a) and HZ-F-20 (b).

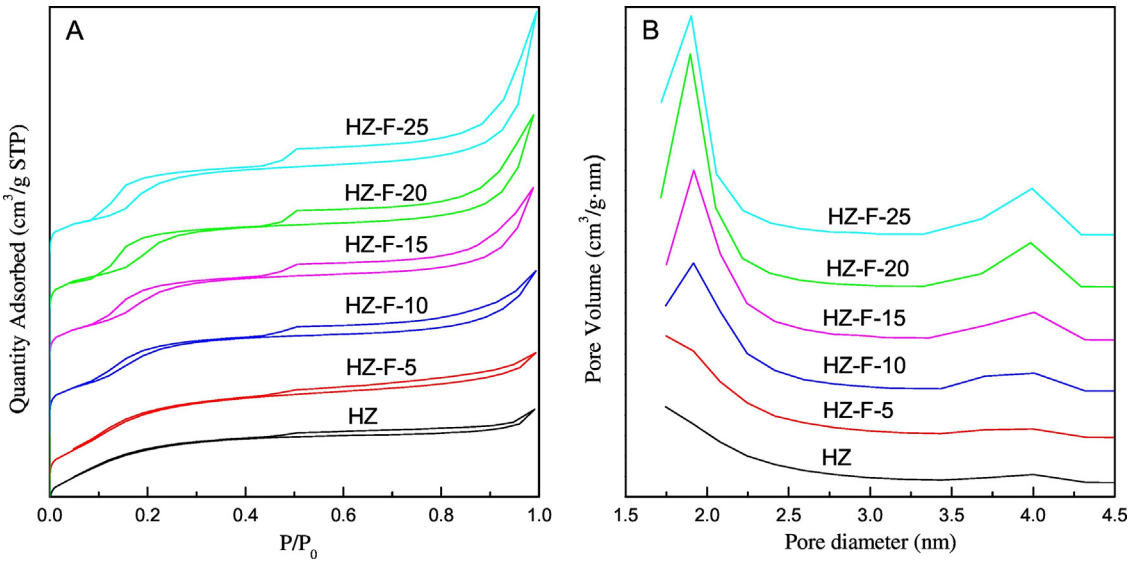

Fig. 3. N_2 physisorption isotherms (A) and pore diameter distributions (B) of different samples.

Moreover, the hysteresis loop of the modified samples became pronounced at high pressure, indicating that the mesopore volume increased distinctly [33] and the mesopores became more abundant with increasing the content of fluorine [31], as evidenced by BJH pore diameter distributions (Fig. 3B). Also, the creation of the new mesopores resulted in larger average pore diameter on the modified samples than the original zeolite HZ, with an increment from 2.30 nm to 3.24 nm (Table 1).

Solid-state ^{27}Al MAS NMR is an effective way to determine the distribution of aluminum among the framework (FAl) and extra-framework (EFAl) sites. For the parent HZSM-5 zeolite, there only appeared two peaks centered at chemical shifts of 54 ppm and 0 ppm (Fig. 4), which can be assigned to tetrahedral FAl and octahedral EFAl [26], respectively. Upon treatment with NH_4F solution, a new aluminum species with the resonance at −14 ppm was found in the fluorinated samples [26], which was assigned to an aluminum hexa-coordinated to oxygen essentially located on the EFAl sites [33]. Furthermore, as the content of F increased, the intensity of the FAl resonance at 54 ppm decreased while that of the EFAl resonances at 0 and −14 ppm increased. At the same time, another peak at around 35 ppm attributed to distorted tetrahedral aluminum in the extra-framework or penta-coordinated aluminum species appeared on the sample of HZ-F-20 and HZ-F-25 [26]. Thereby, it is concluded that partial framework aluminum atoms was extracted becoming extra-framework Al species during the F treatment process. The changes in the distribution of aluminum species would result in a noticeable impact on the acidity thus influencing the catalytic performance of the HZSM-5 zeolite catalysts.

The content of fluorine remaining in fluorine-modified catalysts was detected by EDX, and the results are shown in Table 1. As seen, the measured value of fluorine contents increased apparently from HZ-F-5 to HZ-F-15. This is due to lower levels of fluorine can react adequately with HZSM-5 zeolite, leading to the fluorine remaining in the modified catalysts increased obviously. However, the fluorine contents increased only slightly from HZ-F-15 to HZ-F-25. It may be that the fluorine atoms reacted with HZSM-5 zeolites gradually reached saturation, causing the reaction of fluorine with HZSM-5 zeolites weakened. Thus, the increase of fluorine in the modified catalysts was not obvious.

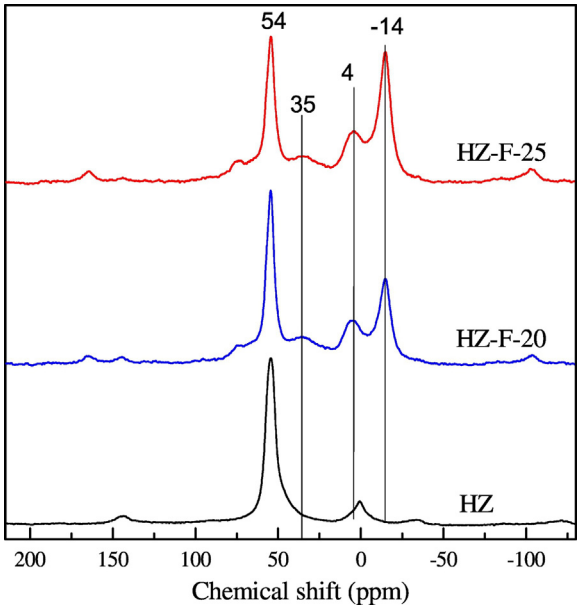

Fig. 4. ^{27}Al MAS NMR spectra of different samples.

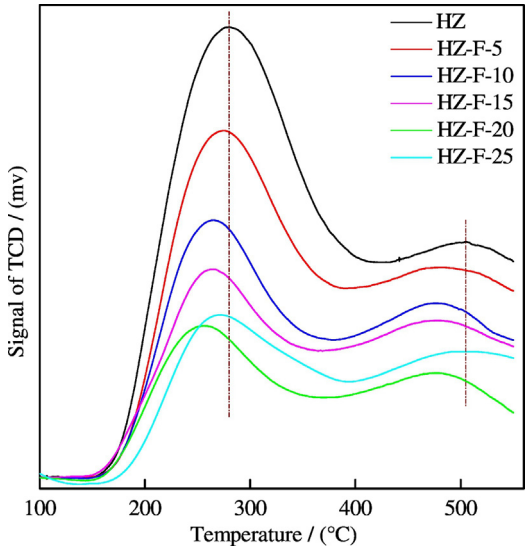

Fig. 5. NH_3-TPD profiles of different samples.

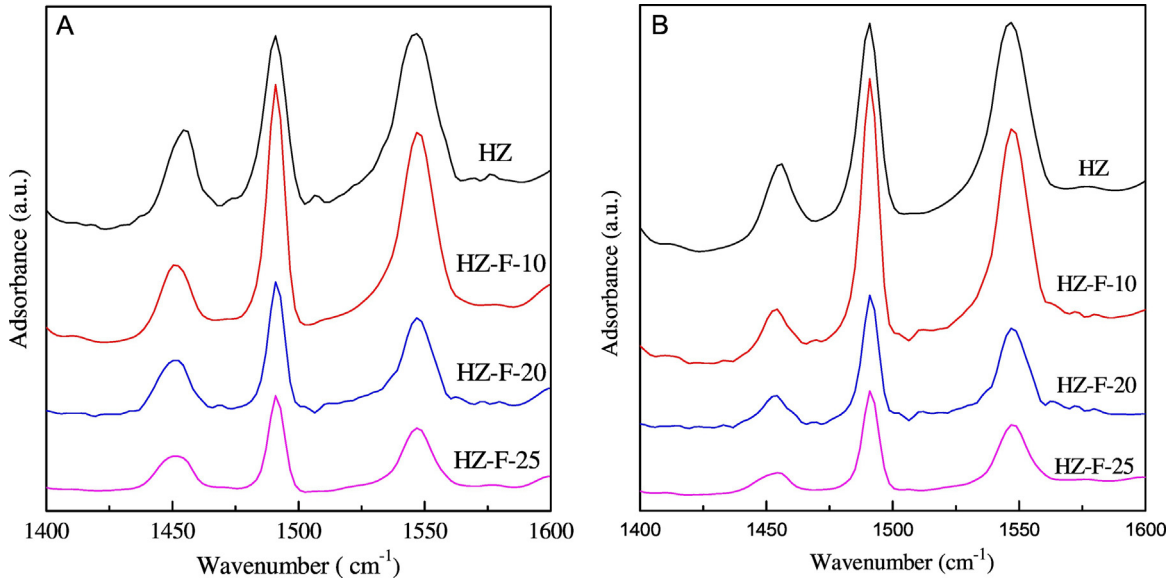

Fig. 6. Py-IR spectra of different samples after desorption at 200 °C (A) and 350 °C (B).

3.1.2. Acidic properties

The acidic properties of the parent and F-modified HZSM-5 catalysts were first studied by NH_3-TPD experiment. As shown in Fig. 5, there are two ammonia desorption peaks located at 200–400 °C and 400–550 °C for all the samples, representing weak acid site and strong acid site, respectively. For the modified samples with fluorine content ≤ 20 wt%, both the strength and concentration of weak acidic sites and strong acidic sites decreased continuously with increasing F contents. This phenomenon may be explained by the deprivation of aluminum from framework [30]. However, the further increase in the fluorine content to 25 wt% led to the enhanced acidity as evidenced by the fact that the two NH_3 desorption peaks of HZ-F-25 shifted to the higher temperatures and their intensity enlarged. It can be attributed to two reasons: on one hand, fluorination would remove aluminum from the framework, leading to more amounts of isolated Al species [34,35]. On the other hand, highly electronegative fluoride ions incorporated into the zeolite framework and polarized the structure [28], leading to the increased surface acidity. As a whole, the effect of fluorine modification on the acidity greatly depends on its content. The lower fluorine content (<20 wt%) leads to the weakened acidity, while the enhanced acidity can be obtained with a higher content (25 wt%).

The acidic properties of the different HZSM-5 catalysts were further characterized by FT-IR of pyridine adsorption. As revealed in Fig. 6, the bands at 1545, 1454, and 1490 cm^{-1} are belonged to the pyridine adsorbed on Brønsted acid sites (B), Lewis acid sites (L) and both acid sites, respectively. The areas of the bands at 1545 and 1454 cm^{-1} were respectively used to calculate the concentrations of B and L acidic sites of different HZSM-5 catalysts [36], and the results are presented in Table 2. As seen, the concentrations of both B and L acid sites decreased progressively with the increase in fluorine content, matching with the results of NH_3-TPD. As B acid sites were closely related to the tetrahedral framework Al, the removal of framework Al as evidenced by ^{27}Al MAS NMR should be responsible for the reduction of B acid sites [33,37]. Meanwhile, the number of L acid sites decreased although more amounts of non-framework Al species were formed. This can be explained by the fact that not all the non-framework Al generates L acid sites [26]. In addition, the B/L ratio (Table 2) at the desorption temperature of 350 °C was higher than that of 200 °C, indicating that more B acid sites occupied in the strong acid sites, while L acid sites accounted for a higher proportion in weak acid sites [25].

Table 2
The amounts of B and L acid sites and their ratios of different HZSM-5 samples.

Sample	A_B (a.u.)		A_L (a.u.)		B/L ratio	
	200 °C	350 °C	200 °C	350 °C	200 °C	350 °C
HZ	4.75	4.44	1.63	0.95	2.91	4.67
HZ-F-10	4.23	3.71	1.17	0.65	3.62	5.71
HZ-F-20	2.00	1.50	1.12	0.46	1.79	3.26
HZ-F-25	1.55	1.19	0.75	0.31	2.07	3.84

According to the above characterization results, the incorporation of F species has a marked effect on acidity of the catalysts. To elucidate the interaction between fluorine and HZSM-5 zeolite, a possible reaction mechanism was supposed in Fig. 7, showing the successive transformations of F modified HZSM-5 zeolite surface with increasing the NH_4F contents.

With the fluorine content ≤ 20 wt%, the possible reactions are as follows: (1) In the process of calcination, HF species were generated by the decomposition of NH_4F and chemisorbed on the zeolite surface in the form of $H^+\cdots F^-$ ion pairs. (2) The zeolite surface reacted with the adsorbed ion pairs ($H^+\cdots F^-$), generating the new hydroxyl groups. (3) During the activation at high temperature (500 °C), surface rearrangement occurred as shown in the following way: F^- transferred to the adjacent Si atom, resulting in a stable Si—F bond. Meanwhile, the electron deficient Si sites were originated by the condensation of the acidic hydroxyl groups. These generated structures have some Lewis acid character as reported elsewhere [29]. As a result, the acidity of F-HZSM-5 zeolites weakened upon the incorporation of F species.

However, when the content of fluorine increased to 25 wt%, the ion pairs ($H^+\cdots F^-$) could further react with the new structure generated by surface rearrangement and form the silanol groups, enhancing the surface acidity. Therefore, the acidity of catalysts strengthened in some degree by the higher fluorine content.

In summary, the interaction between fluorine and zeolite framework vary with increasing the NH_4F concentrations. It is this interaction that leads to the change of surface acidity of F modified HZSM-5 catalysts.

3.2. Catalytic performance

3.2.1. Effect of fluorine modification on product selectivity

The selective conversion of bio-ethanol into propene was performed on the parent and F-modified HZSM-5 zeolite catalysts at 500 °C,

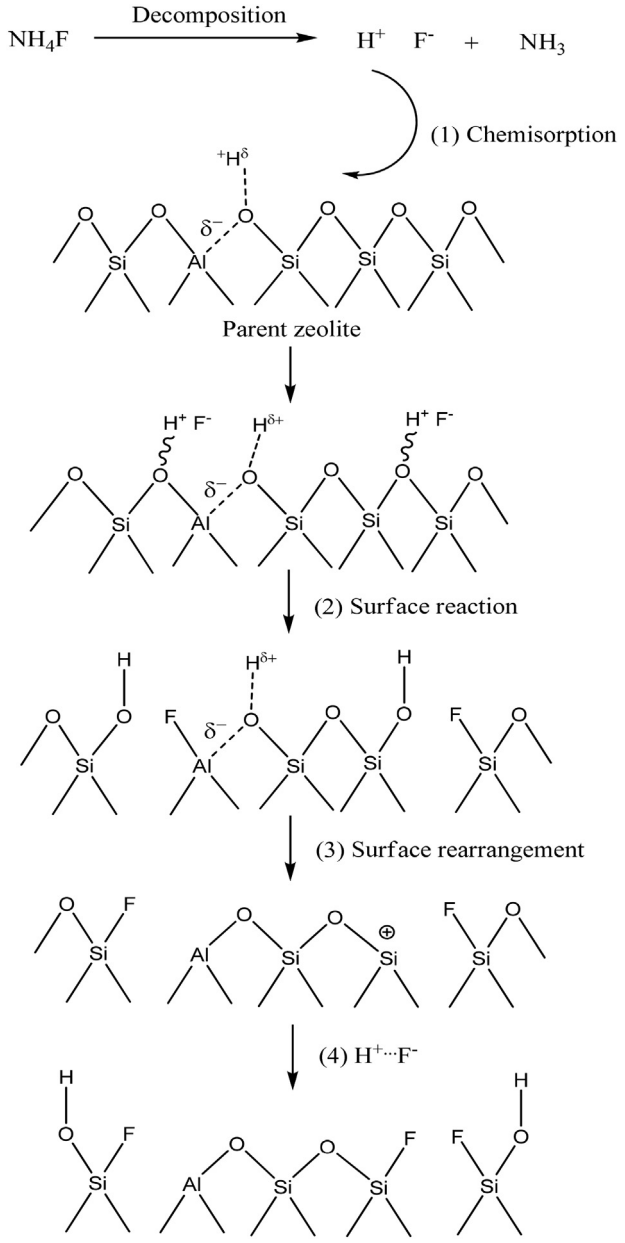

Fig. 7. Supposed interaction of fluorine with the zeolite framework.

atmospheric pressure, and WHSV of 10 h^{-1}, and the conversion of ethanol maintained 100% during the whole reaction process. The reaction products are divided into light olefins (ethene, propene, and butene), C_{1-4} paraffins (methane, ethane, propane, and butane), aliphatics (C_{5+}), and aromatics, and the results of the initial product distributions are summarized in Table 3.

Table 3
Product selectivity on different HZSM-5 catalysts for the conversion of bio-ethanol to propene.

Sample	Distribution of products (mol%)				
	Ethene	Propene	Butene	Paraffins (C_{1-4}) + aliphatics (C_{5+})	Aromatics
HZ	5.9	7.3	5.6	45.5	35.7
HZ-F-5	12.4	16.4	9.7	37.5	24.0
HZ-F-10	17.5	21.2	9.5	37.6	14.1
HZ-F-15	19.1	21.5	9.6	33.1	16.7
HZ-F-20	21.9	21.4	8.6	33.1	15.0
HZ-F-25	29.5	22.5	7.5	29.8	10.7

Reaction conditions: 500 °C, atmospheric pressure, ethanol/water = 9/1 vol/vol, and WHSV of ethanol = 10 h^{-1}.

As shown in Table 3, the initial selectivity of different products varies from different HZSM-5 catalysts. Specifically, the ethene selectivity over the F-modified HZSM-5 catalysts was larger than that on the parent HZ sample and increased gradually with the increase of fluorine content. On the contrary, the selectivity of C_{1-4} paraffins, C_{5+} aliphatics, and aromatics decreased after F modification. On the other hand, the selectivity of propene and butene increased noticeably after F modification but exhibited little difference among the different F-modified samples. The changes of products distribution over different catalysts can be attributed to the changes of acidity and pore structure induced by fluorine modification. According to NH_3-TPD results, both the concentrations and strength of acid sites deceased after fluorine modification and gradually with the increase of fluorine content. Previous investigations showed that more ethene was formed with lower surface acidity [10], and the reduction of the amount of strong acid sites favored the improvement of propene selectivity [38]. Thus, the fluorinated samples exhibited higher light olefins (C_2–C_4) selectivity. However, the production of C_{1-4} paraffins, C_{5+} aliphatics and aromatics by hydrogenation as well as oligomerization-cracking, aromatization, and hydrogen transfer requires high surface acidity [16]. Consequently, the selectivity of C_{1-4} paraffins, C_{5+} aliphatics and aromatics gradually reduced with the decreased surface acidity by fluorine modification. On the other hand, although possessing higher acidity compared with HZ-F-20, the HZ-F-25 sample exhibited lower selectivity to paraffins, C_{5+} aliphatics and aromatics, which can be probably attributed to the enlarged pore size of the HZ-F-25 sample (Table 1). Based on the reaction pathways (Fig. 8) supposed for the ETP process [12,39,40], B acid sites are the active sites for the conversion of ethanol to propene [41,42]. Firstly, ethene was produced from ethanol, and then the ethene was converted in parallel to propene and butene. Finally, propene and butene were converted to propane, butane, and other higher hydrocarbons such as paraffins and aromatics. The large pore size would promote the diffusion of the propene and butene out of the channels, reducing their contact time with the active acid sites. Thus, the formation of the paraffins, C_{5+} aliphatics and aromatics would be efficiently inhibited [43]. This result suggests that the selectivity of products is simultaneously dependent on the acidic and textural properties of the HZSM-5 zeolite catalysts.

3.2.2. Effect of fluorine modification on catalyst stability

The effect of time on stream (TOS) on the selectivity of C_2–C_4 olefins (ethene, propene, and butylene) and aromatics was investigated for the selective conversion of bio-ethanol to propene and the results are presented in Fig. 9. As shown, the ethene selectivity of all the samples increased continuously with TOS. In contrast, the aromatics selectivity decreased with reaction time. As pointed by Song et al. [38] and Inoue et al. [44], low surface acidity favored the formation of ethene, while high surface acidity led to the formation of more aromatics. As the reaction progressed, coke formed and covered the strong acidic sites preferentially [6]. Thus, ethene can still be formed by ethanol dehydration on weak acidic sites, while the generation of aromatics cannot occur for the requirement of higher acidity. Therefore, the changing trend of selectivity to ethene and aromatics can be reasonably ascribed to the deactivation of the strong acidic sites [10], which was evidenced by NH_3-TPD measurement (see below).

As shown in Fig. 9(B) and (C), the selectivity of propene and butene showed a similar changing trend, i.e. increased firstly, passed through a maximum, and then decreased. This phenomenon suggests that propene and butene are produced by the parallel pathways and the common intermediate on the HZSM-5 zeolites [6]. Moreover, the variation trend of selectivity to propene and butene with TOS can also be explained based on the proposed reaction pathways [12,39,40]. First, ethene was formed by dehydration of ethanol (step 1), and then ethene converted to propene and butene (step 2). Finally, i.e. step 3, propene and butene oligomerized to higher olefins, aromatics and coke. As the

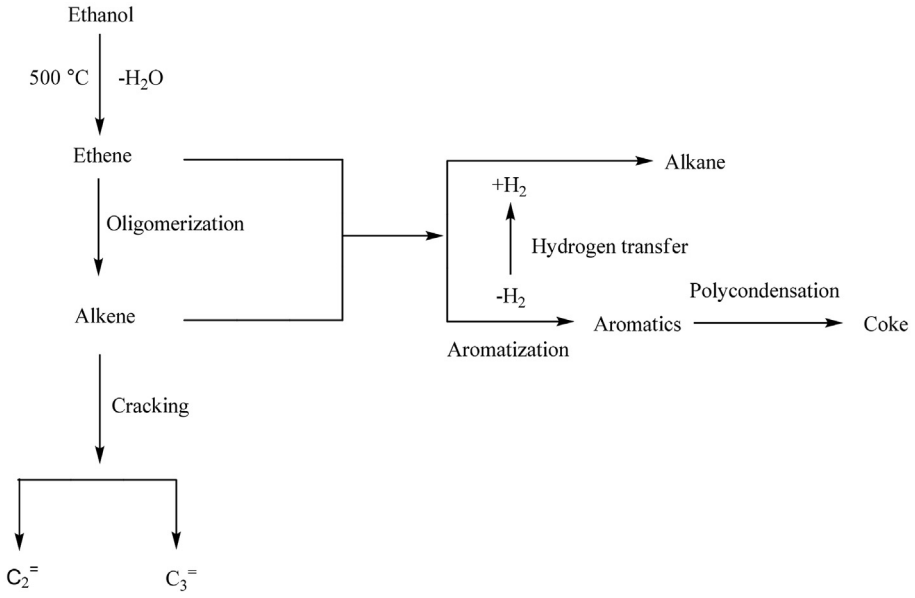

Fig. 8. Supposed reaction pathways for ethanol conversion at high temperature.

reaction proceeded, the strongest acid sites preferentially deactivated by coke affected the conversion of light olefins into higher hydrocarbons (step 3), reducing the consumption of propene and butene, and subsequently the medium strong acid sites required in the step 2 was also deactivated by coke. Therefore, the selectivity of propene and butene increased first and then decreased [12].

Although the variation trend of propene selectivity was similar among all the samples, their change rates of propene selectivity were greatly different. For the parent HZ, the initial propene selectivity was the lowest, reaching a maximum value (20.2%) at 16 h, and then falling below 10% after 38 h. The similar trends were observed for the fluorinated samples. However, the initial propene selectivity was much higher, and the catalytic stability was also improved compared to the parent HZ. The advantages were even more pronounced for the HZ-F-20 catalyst: the highest propene selectivity reached at 24.9% after 9 h, and the catalyst life (the reaction time for the propene selectivity maintained at ≥10%) extended substantially to 214 h, even more than five times longer than that of the original catalyst HZ. The propene selectivity on all the catalysts in the long run followed the sequence of HZ-F-20 > HZ-F-15 > HZ-F-25 > HZ-F-10 > HZ-F-5 > HZ. Apparently, the HZ-F-20 catalyst exhibited the optimal performance for the stable production of propene from bio-ethanol.

In order to elucidate the origin of the significant improvement of the stability of the F-modified catalysts especially HZ-F-20 compared to the parent HZ, the spent catalysts were characterized by several techniques. As the spent catalysts were black in color, carbon deposition may be the main cause for the drop of propene selectivity [45,46]. Therefore, the spent catalysts were first investigated by TG analysis. As shown in Fig. 10, there is an obvious weight loss in 400–700 °C, indicating the vigorous combustion of coke on all the spent HZSM-5 catalysts. The relative amounts of carbonaceous deposits for the spent HZ, HZ-F-5, HZ-F-10, HZ-F-15, HZ-F-20, and HZ-F-25 were 7.5%/39 h, 7.1%/63 h, 8.8%/101 h, 12.6%/128 h, 16.1%/214 h and 10.5%/128 h, respectively. Combining the catalytic testing results (Fig. 9), it can be inferred that the F-modified HZSM-5 catalysts especially HZ-F-20 had a significantly enhanced ability to tolerate the coke deposits.

On the other hand, the average carbon deposition rate on HZ, HZ-F-5, HZ-F-10, HZ-F-15, HZ-F-20, and HZ-F-25 were 1.9×10^{-3}, 1.1×10^{-3}, 8.7×10^{-4}, 9.8×10^{-4}, 7.5×10^{-4}, and 8.2×10^{-4} $g/g_{cat}h$, respectively. The result showed that the coking rate of the HZSM-5 zeolite catalyst decreased dramatically by fluorine modification, and it was especially pronounced for the HZ-F-20 catalyst (less half of the parent HZ). As reported by Sun et al. [47], the coking rate was affected by both acidity (especially the amount of strong B acid sites) and the microporous diffusibility. According to the above NH_3-TPD and Py-IR characterization results, fluorine modification notably reduced the amount of strong B acid sites and consequently the carbon deposition rate declined significantly. On the other hand, the N_2 adsorption characterization results showed that fluorine treatment increased the amount of mesopores, which may establish the interconnected mesoporous-microporous network to reduce the diffusion path length. The shorter the paths were, the easier coke precursors would reach the external surface, thus reducing the chance of coke formation.

Since the coke formation mainly occurs in the secondary pores of the HZSM-5 zeolite catalysts in the ethanol conversion process [8,10], the pore properties of the spent catalysts were characterized by N_2 physisorption. As shown in Fig. 11(A), the hysteresis loops of the spent catalysts especially HZ-F-20-S was distinctly smaller than those of the fresh catalysts. Also, as shown in Fig. 11(B), the pore size distribution curves of the spent catalysts were very different from those of the fresh samples, suggesting that a majority of mesopores of the catalysts were blocked by coking.

The textural properties of the spent samples as well as the corresponding fresh ones for the sake of comparison are summarized in Table 4. Clearly, after the reaction, the BET surface areas of the both catalysts were significantly decreased and the reduction was mainly caused by the decrease in the external surface area. This result further confirmed that coking mainly occurred on the external surface of HZSM-5 zeolite [38].

Fig. 12 shows the NH_3-TPD profiles of HZ and HZ-F-20 before and after reaction. Clearly, the amount of acid sites of HZ-S reduced remarkably and the NH_3-desorption peak at about 275 °C shifted to low temperature, indicating that the acidity weakened considerably. Notably, all the NH_3-desorption peaks of HZ-F-20-S almost disappeared. Combined with the performance of the catalyst (Fig. 9), it was found that the HZ-F-20-S sample which has lost almost all the acidity still catalyze the dehydration of ethanol to ethene and the further conversion of ethene to other hydrocarbons. Similar phenomenon was also reported by other researchers [48].

Besides coke deposit, the removal of framework aluminum may be another important reason for deactivation of the HZSM-5 catalyst during the selective conversion of bio-ethanol to propene at high temperature [38]. In this case, the structure of the HZSM-5 zeolite was destroyed, and the catalytic performance cannot be recovered totally

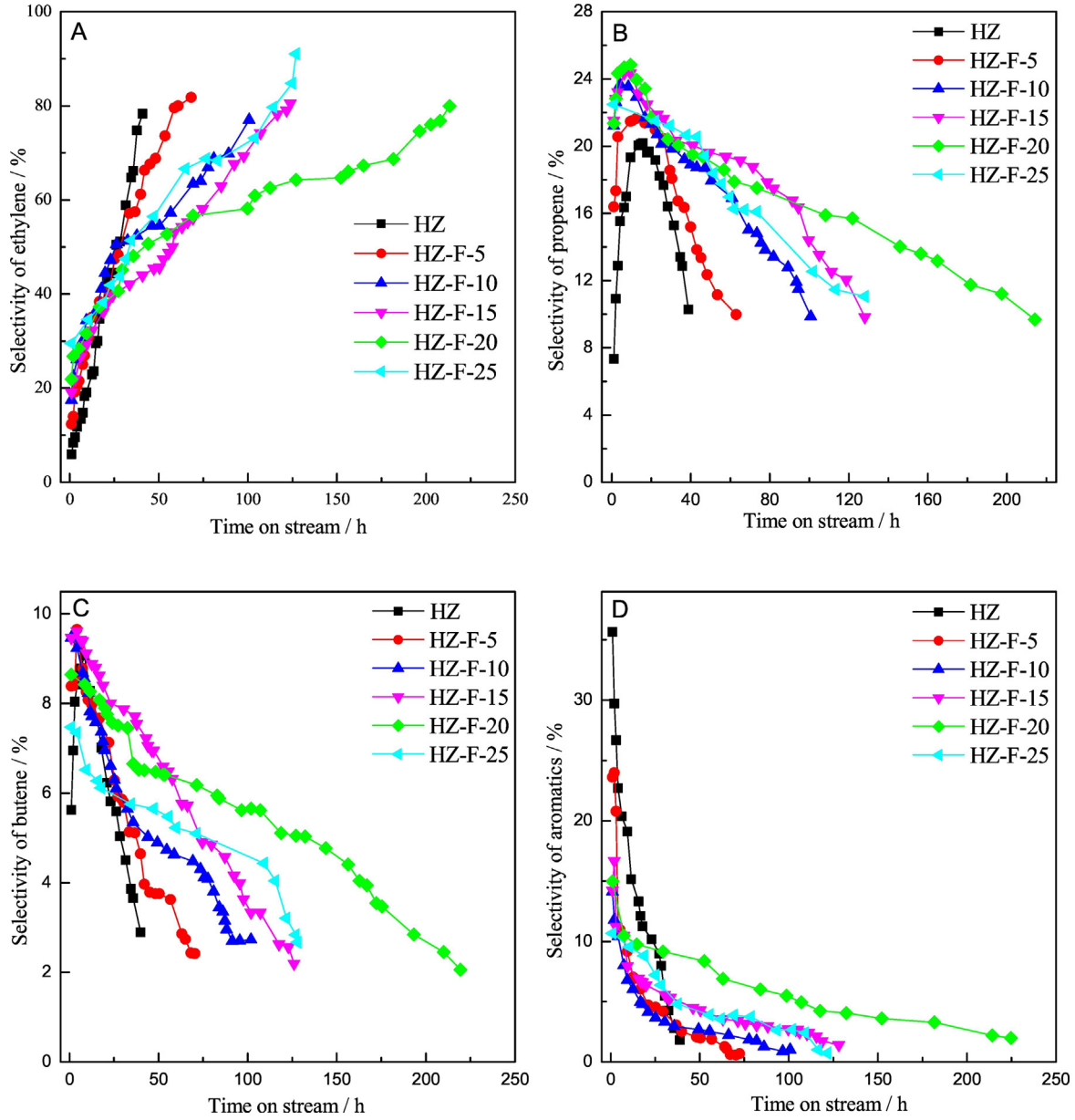

Fig. 9. Effect of time on stream on selectivity of C_2–C_4 olefins and aromatics over different HZSM-5 zeolites. Reaction conditions: 500 °C, atmospheric pressure, ethanol/water = 9/1 vol/vol, and WHSV of ethanol = 10 h^{-1}.

by regeneration. Since the initial propene selectivity of the regenerated catalysts (by calcining in air at 550 °C for 2 h) was not totally recovered and decreased more rapidly with TOS than the fresh samples, it is inferred that the irreversible deactivation by framework collapse of the HZSM-5 zeolite occurred during the reaction [6,18].

In order to confirm the hypothesis of framework collapse [49–51], XRD measurements were carried out. Fig. 13 shows XRD patterns of HZ and HZ-F-20 before and after reaction. As shown in Fig. 13(B), the two peaks at about 23° in the fresh catalysts were changed into a single peak after deactivation. As all XRD peaks are due to the framework of zeolite HZSM-5, the reduction of the diffraction peaks suggests the framework damage, at least in part, during the reaction. Moreover, the relative crystallinity before and after reaction calculated by the diffraction peaks detected in the range of 22–25° is summarized in Table 4, showing that the relative crystallinity decreased obviously for both HZ-S and HZ-F-20-S compared with their fresh ones. Therefore, it can be concluded that framework collapse by dealumination occurred in reaction process for both catalysts.

Based on the above characterization results of the spent catalysts, it can be concluded that there are two possible reasons for the improvement of the catalytic stability by fluorine modification. One is the decreased acidity. It is clear that the concentration of strong B acid sites is closely related to the formation of coke [52], which makes the catalyst deactivate fast. The attenuated acidity slows down the coking rate, thus prolonging the catalyst lifetime. The other reason might be the improved pore structure. The enlarged external surface area and pore volume enhance the tolerance capacity to coke, and the improved diffusion performance suppresses the generation of the coke. Therefore, the catalytic stability of HZSM-5 zeolite was improved greatly after F modification.

4. Conclusions

Fluorination of nano-HZSM-5 by NH_4F solution maintained the HZSM-5 zeolite structure, with a consequent increase of external area, mesoporous volume and pore diameter. When the fluorine content

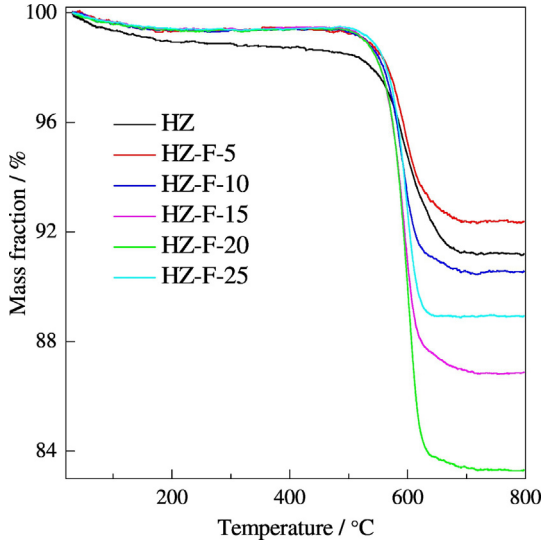

Fig. 10. TG curves of different spent HZSM-5 samples.

was ≤20 wt%, both the amount and strength of the acid sites on the surface of modified HZSM-5 zeolite decreased with increasing the fluorine contents. However, the extortionate fluorine content (25 wt%) could lead to a slightly stronger acidity on account of the inductive effect of fluoride ions, confirming that fluorine atoms were introduced into the zeolite framework.

The selective conversion of bio-ethanol to propene was implemented on the parent and modified nano-HZSM-5 catalysts. The fluorine modified catalyst with appropriate amount (20 wt%) showed higher initial propene selectivity and significantly longer lifetime than the parent sample, which can be attributed to its weakened acidity, larger external surface area and more secondary pores. The attenuated acidity contributed to lower the formation rate of coke, and the optimization of the pore structure not only reduced the diffusion limitation of the products, thus markedly decreasing the coking rate, but also provided more space for accommodating the coke deposits, thus significantly improving the tolerance capacity to coke deposit. Besides the coke deposits, structure degradation of zeolite due to elimination of aluminum in the zeolite framework was also an important reason for the deactivation of the parent and fluorinated nano-HZSM-5 zeolite catalysts.

Table 4
Textural properties and relative crystallinity of the fresh and spent HZSM-5 samples.

Sample	Surface area ($m^2\ g^{-1}$)			Pore volume ($cm^3\ g^{-1}$)			D_p[a] (nm)	RC[b] (%)
	Total	Micropore	External	Total	Micropore	Mesopore		
HZ	326	226	100	0.19	0.12	0.07	2.30	100
HZ-S[c]	243	193	50	0.13	0.10	0.03	2.22	88
HZ-F-20	340	68	272	0.25	0.04	0.21	2.88	85
HZ-F-20-S[d]	233	165	68	0.17	0.08	0.09	2.96	57

[a] Average pore diameter.
[b] Relative crystallinity calculated from XRD patterns.
[c] Time on stream of HZ-S: 39 h.
[d] Time on stream of HZ-F-20-S: 214 h.

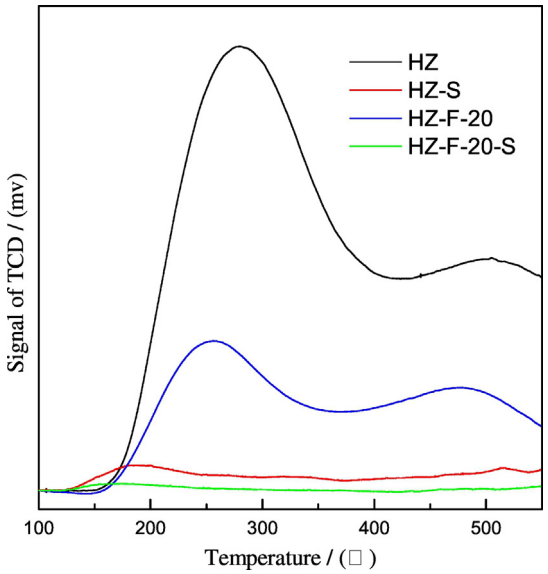

Fig. 12. NH_3-TPD profiles of the fresh and spent HZSM-5 samples. (Time on stream: HZ-S = 39 h, HZ-F-20-S = 214 h).

Acknowledgement

The authors thank Shanghai Municipal Education Commission (J51503) for financial support.

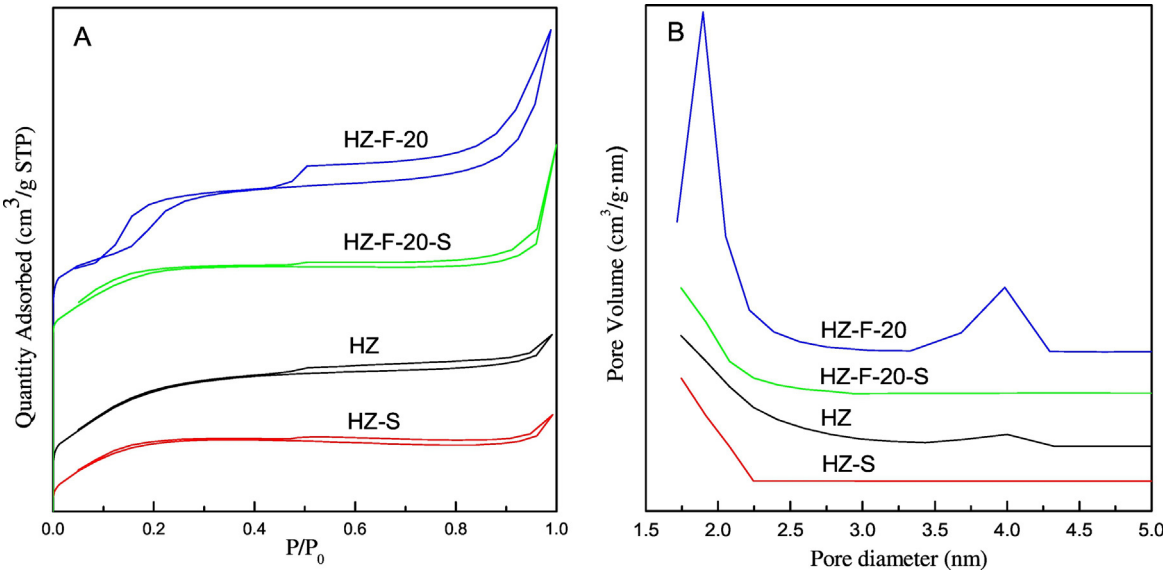

Fig. 11. N_2 physisorption isotherms (A) and pore diameter distribution (B) of the fresh and spent HZSM-5 samples. (Time on stream: HZ-S = 39 h, HZ-F-20-S = 214 h).

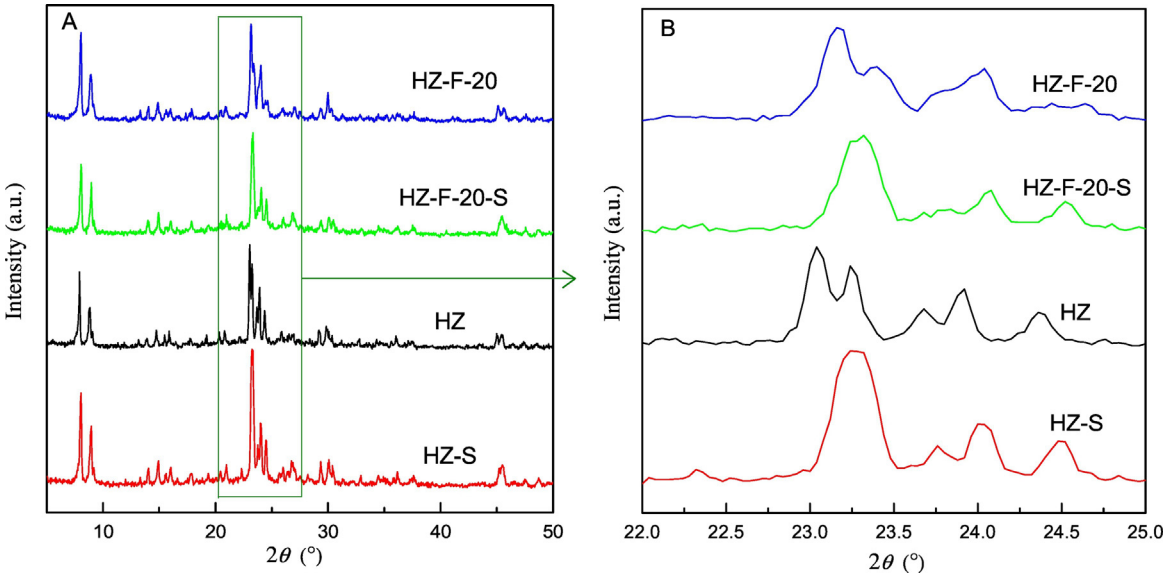

Fig. 13. XRD patterns of the fresh and spent HZSM-5 samples. (Time on stream: HZ-S = 39 h, HZ-F-20-S = 214 h).

References

[1] M. Iwamoto, Selective catalytic conversion of bio-ethanol to propene: a review of catalysts and reaction pathways, Catal. Today 242 (2015) 243–248.
[2] Y. Furumoto, Y. Harada, N. Tsunoji, A. Takahashi, T. Fujitani, Y. Ide, M. Sadakane, T. Sano, Effect of acidity of ZSM-5 zeolite on conversion of ethanol to propylene, Appl. Catal. A Gen. 399 (2011) 262–267.
[3] J. Sun, Y. Wang, Recent advances in catalytic conversion of ethanol to chemicals, ACS Catal. 4 (2014) 1078–1090.
[4] X. Li, A. Kant, Y. He, H.V. Thakkar, M.A. Atanga, F. Rezaei, D.K. Ludlow, A.A. Rownaghi, Light olefins from renewable resources: selective catalytic dehydration of bioethanol to propylene over zeolite and transition metal oxide catalysts, Catal. Today 276 (2016) 62–77.
[5] K.K. Ramasamy, H. Zhang, J. Sun, Y. Wang, Conversion of ethanol to hydrocarbons on hierarchical HZSM-5 zeolites, Catal. Today 238 (2014) 103–110.
[6] J.J. Huangfu, D.S. Mao, X.L. Zhai, Q.S. Guo, Remarkably enhanced stability of HZSM-5 zeolite co-modified with alkaline and phosphorous for the selective conversion of bio-ethanol to propylene, Appl. Catal. A Gen. 520 (2016) 99–104.
[7] A.G. Gayubo, A. Alonso, B. Valle, A.T. Aguayo, J. Bilbao, Selective production of olefins from bioethanol on HZSM-5 zeolite catalysts treated with NaOH, Appl. Catal. B Environ. 97 (2010) 299–306.
[8] Q. Sheng, K. Ling, Z. Li, L. Zhao, Effect of steam treatment on catalytic performance of HZSM-5 catalyst for ethanol dehydration to ethylene, Fuel Process. Technol. 110 (2013) 73–78.
[9] J. Bi, X. Guo, M. Liu, X. Wang, High effective dehydration of bio-ethanol into ethylene over nanoscale HZSM-5 zeolite catalysts, Catal. Today 149 (2010) 143–147.
[10] T. Meng, D.S. Mao, Q.S. Guo, G.Z. Lu, The effect of crystal sizes of HZSM-5 zeolites in ethanol conversion to propylene, Catal. Commun. 21 (2012) 52–57.
[11] N. Viswanadham, S.K. Saxena, J. Kumar, P. Sreenivasulu, D. Nandan, Catalytic performance of nano crystalline H-ZSM-5 in ethanol to gasoline, Fuel 95 (2012) 298–304.
[12] Y. Takamitsu, K. Yamamoto, S. Yoshida, H. Ogawa, T. Sano, Effect of crystal size and surface modification of ZSM-5 zeolites on conversion of ethanol to propylene, J. Porous. Mater. 21 (2014) 433–440.
[13] L. Lakiss, F. Ngoye, C. Canaff, S. Laforge, Y. Pouilloux, Z.X. Qin, M. Tarighi, K. Thomas, V. Valtchev, A. Vicente, L. Pinard, J.-P. Gilson, C. Fernandez, On the remarkable resistance to coke formation of nanometer-sized and hierarchical MFI zeolites during ethanol to hydrocarbons transformation, J. Catal. 328 (2015) 165–172.
[14] J.D. Bi, M. Liu, C.S. Song, X.S. Wang, X.W. Guo, C_2–C_4 light olefins from bioethanol catalyzed by Ce-modified nanocrystalline HZSM-5 zeolite catalysts, Appl. Catal. B Environ. 107 (2011) 68–76.
[15] D. Goto, Y. Harada, Y. Furumoto, A. Takahashi, T. Fujitani, Y. Oumi, M. Sadakane, T. Sano, Conversion of ethanol to propylene over HZSM-5 type zeolites containing alkaline earth metals, Appl. Catal. A Gen. 383 (2010) 89–95.
[16] Z. Song, A. Takahashi, N. Mimura, T. Fujitani, Production of propylene from ethanol over ZSM-5 zeolites, Catal. Lett. 131 (2009) 364–369.
[17] Z. Song, A. Takahashi, I. Nakamura, T. Fujitani, Phosphorus-modified ZSM-5 for conversion of ethanol to propylene, Appl. Catal. A Gen. 384 (2010) 201–205.
[18] A. Takahashi, W. Xia, I. Nakamura, H. Shimada, T. Fujitani, Effects of added phosphorus on conversion of ethanol to propylene over ZSM-5 catalysts, Appl. Catal. A Gen. 423-424 (2012) 162–167.
[19] C. Duan, X. Zhang, R. Zhou, Y. Hua, L. Zhang, J. Chen, Comparative studies of ethanol to propylene over HZSM-5/SAPO-34 catalysts prepared by hydrothermal synthesis and physical mixture, Fuel Process. Technol. 108 (2013) 31–40.
[20] C. Duan, Y. Hua, X. Zhang, J. Chen, R. Zhou, L. Zhang, Hydrothermally synthesized HZSM-5/SAPO-34 composite zeolite catalyst for ethanol conversion to propylene, Catal. Lett. 141 (2011) 1821–1827.
[21] M.D. González, P. Salagre, M. Linares, R. García, D. Serrano, Y. Cesteros, Effect of hierarchical porosity and fluorination on the catalytic properties of zeolite beta for glycerol etherification, Appl. Catal. A Gen. 473 (2014) 75–82.
[22] L. Wang, F. Wang, J. Wang, Catalytic properties of Pd/HY catalysts modified with NH_4F for acetylene hydrochlorination, Catal. Commun. 65 (2015) 41–45.
[23] Q. Yang, M. Kong, Z.Y. Fan, X.J. Meng, J.H. Fei, F.S. Xiao, Aluminum fluoride modified HZSM-5 zeolite with superior performance in synthesis of dimethyl ether from methanol, Energy Fuel 26 (2012) 4475–4480.
[24] X. Feng, G.Y. Jiang, Z. Zhao, L. Wang, X.H. Li, A.J. Duan, J. Liu, C.M. Xu, J.S. Gao, Highly effective F-modified HZSM-5 catalysts for the cracking of naphtha to produce light olefins, Energy Fuel 24 (2010) 4111–4115.
[25] Q.S. Guo, D.S. Mao, Y.P. Lao, G.Z. Lu, The effect of fluorine modification on catalytic performance of nanosized HZSM-5 zeolite for conversion of methanol to propene, Chin. J. Catal. 30 (2009) 1248–1254.
[26] Y.N. Wang, X.W. Guo, C. Zhang, F.L. Song, X.S. Wang, H.O. Liu, X.C. Xu, C.S. Song, W.P. Zhang, X.M. Liu, X.W. Han, X.H. Bao, Influence of calcination temperature on the stability of fluorinated nanosized HZSM-5 in the methylation of biphenyl, Catal. Lett. 107 (2006) 209–214.
[27] Y.Q. Song, Y.L. Feng, F. Liu, C.L. Kang, X.L. Zhou, L.Y. Xu, G.X. Yu, Effect of variations in pore structure and acidity of alkali treated ZSM-5 on the isomerization performance, J. Mol. Catal. A Chem. 310 (2009) 130–137.
[28] Z. Qin, L. Lakiss, J.-P. Gilson, K. Thomas, J.-M. Goupil, C. Fernandez, V. Valtchev, Chemical equilibrium controlled etching of MFI-type zeolite and its influence on zeolite structure, acidity, and catalytic activity, Chem. Mater. 25 (2013) 2759–2766.
[29] R. Le Van Mao, T.S. Le, M. Fairbairn, A. Muntasar, S. Xiao, G. Denes, ZSM-5 zeolite with enhanced acidic properties, Appl. Catal. A 185 (1999) 41–52.
[30] X.F. Zhang, R.J. Wang, X.X. Yang, Effect of alkaline treatment on pore structure and acidity of HZSM-5 in the synthesis of ethyl mercaptan, Catal. Commun. 60 (2015) 32–36.
[31] Z.J. Hu, H.B. Zhang, L. Wang, H.X. Zhang, Y.H. Zhang, H.L. Xu, W. Shen, Y. Tang, Highly stable boron-modified hierarchical nanocrystalline ZSM-5 zeolite for the methanol to propylene reaction, Catal. Sci. Technol. 4 (2014) 2891–2895.
[32] J. Groen, Critical appraisal of mesopore characterization by adsorption analysis, Appl. Catal. A Gen. 268 (2004) 121–125.
[33] J.M. Müller, G.C. Mesquita, S.M. Franco, L.D. Borges, J.L. de Macedo, J.A. Dias, S.C.L. Dias, Solid-state dealumination of zeolites for use as catalysts in alcohol dehydration, Microporous Mesoporous Mater. 204 (2015) 50–57.
[34] N.A. Sánchez, J.M. Saniger, J.-B. d'Espinose de la Caillerie, A.L. Blumenfeld, J.J. Fripiat, Reaction of HY zeolite with molecular fluorine, J. Catal. 201 (2001) 80–88.
[35] V.G. Alexander, G. Panov, J.J. Fripiat, Fluorination of USY and modification of its catalytic properties, J. Catal. 168 (1997) 321–327.
[36] D.S. Mao, W.M. Yang, J.C. Xia, B. Zhang, Q.Y. Song, Q.L. Chen, Highly selective hybrid catalyst for the direct synthesis of dimethyl ether from syngas with magnesium oxide-modified HZSM-5 as a dehydration component, J. Catal. 230 (2005) 140–149.
[37] Z.J. Wan, W. Wu, W. Chen, H. Yang, D.K. Zhang, Direct synthesis of hierarchical ZSM-5 zeolite and its performance in catalyzing methanol to gasoline conversion, Ind. Eng. Chem. Res. 53 (2014) 19471–19478.
[38] Z. Song, W. Liu, C. Chen, A. Takahashi, T. Fujitani, Production of propylene from ethanol over ZSM-5 co-modified with zirconium and phosphorus, React. Kinet. Mech. Catal. 109 (2013) 221–231.

[39] A. Takahashi, W. Xia, Q. Wu, T. Furukawa, I. Nakamura, H. Shimada, T. Fujitani, Difference between the mechanisms of propylene production from methanol and ethanol over ZSM-5 catalysts, Appl. Catal. A Gen. 467 (2013) 380–385.
[40] M. Inaba, K. Murata, M. Saito, I. Takahara, Ethanol conversion to aromatic hydrocarbons over several zeolite catalysts, React. Kinet. Catal. Lett. 88 (2006) 135–141.
[41] S. Bun, S. Nishiyama, S. Tsuruya, M. Masai, Ethanol conversion over ion-exchanged ZSM-5 zeolites, Appl. Catal. 59 (1990) 13–29.
[42] K. Murata, M. Inaba, I. Takahara, Effects of surface modification of H-ZSM-5 catalysts on direct transformation of ethanol into lower olefins, J. Jpn. Pet. Inst. 51 (2008) 234–239.
[43] W. Xia, K. Chen, A. Takahashi, X. Li, X. Mu, C. Han, L. Liu, I. Nakamura, T. Fujitani, Effects of particle size on catalytic conversion of ethanol to propylene over H-ZSM-5 catalysts—smaller is better, Catal. Commun. 73 (2016) 27–33.
[44] K. Inoue, K. Okabe, M. Inaba, I. Takahara, K. Murata, Metal modification effects on ethanol conversion to propylene by H-ZSM-5 with Si/Al_2 ratio of 150, React. Kinet. Mech. Catal. 101 (2010) 477–489.
[45] L. Pinard, K. Ben Tayeb, S. Hamieh, H. Vezin, C. Canaff, S. Maury, O. Delpoux, Y. Pouilloux, On the involvement of radical “coke” in ethanol conversion to hydrocarbons over HZSM-5 zeolite, Catal. Today 218-219 (2013) 57–64.
[46] F. Wang, T. Bai, C. Duan, W.T. Qu, X.L. Liu, X. Zhang, Coke on HZSM-5/SAPO-34 catalyst for ethanol to propylene, Adv. Mater. Res. 962-965 (2014) 751–754.
[47] L. Sun, X. Wang, J. Li, A. Ma, H. Guo, Effect of acidity and diffusibility on coke deactivation over nano-sized HZSM-5 zeolites, React. Kinet. Mech. Catal. 102 (2010) 235–247.
[48] F. Ferreira Madeira, N.S. Gnep, P. Magnoux, H. Vezin, S. Maury, N. Cadran, Mechanistic insights on the ethanol transformation into hydrocarbons over HZSM-5 zeolite, Chem. Eng. J. 161 (2010) 403–408.
[49] M. Inaba, K. Murata, I. Takahara, K. Inoue, Production of olefins from ethanol by Fe and/or P-modified H-ZSM-5 zeolite catalysts, J. Chem. Technol. Biotechnol. 86 (2011) 95–104.
[50] M. Inaba, K. Murata, M. Saito, I. Takahara, Production of olefins from ethanol by Fe-supported zeolite catalysts, Green Chem. 9 (2007) 638–646.
[51] M. Inaba, K. Murata, I. Takahara, K. Inoue, Production of C_{3+} olefins and propylene from ethanol by Zr-modified H-ZSM-5 zeolite catalysts, Adv. Mater. Sci. Eng. 2012 (2012) 1–7.
[52] T. Bai, X. Zhang, F. Wang, W. Qu, X. Liu, C. Duan, Coking behaviors and kinetics on HZSM-5/SAPO-34 catalysts for conversion of ethanol to propylene, J. Energy Chem. 25 (2016) 545–552.